SSRG International Journal of Mechanical Engineering
ISSN: 2348-8360/ https://doi.org/10.14445/23488360/IJME-V11I12P103

Volume 11 Issue 12, 29-37, December 2024

Original Article

Design of Direct Heating Thermal Dryer using Mineral Insulated Cable for Lithium Hydroxide Processing

Han-So Lee[1], Jyun-Pyo Hong[1], Jung-Woo Song[1], Jong-Hun Kang[2]

[1]*Department of Convergence Engineering, Jungwon University, Republic of Korea.*
[2]*Department of Aero Mechanical Engineering, Jungwon University, Republic of Korea.*

[2]*Corresponding Author : jhkang@jwu.ac.kr*

Received: 07 October 2024 Revised: 17 November 2024 Accepted: 04 December 2024 Published: 27 December 2024

Abstract *- The present study is about designing a direct heating dryer for drying secondary battery cathode materials. An efficient heating analysis method was proposed to evaluate the temperature, deformation, and stress of dryer components when increasing the dryer temperature using the direct heating method. The heating temperature of the thermal dryer was set to 250 °C, 300 °C, and 350 °C, and the temperature distribution was investigated through the heating analysis of the dryer, and its deformation and stress due to the high temperature were analyzed. The structural analysis confirmed that plastic deformation occurred at all of 250 °C, 300 °C, and 350 °C, as the yield strength was exceeded. Since the deformation and stress were repeated according to the reciprocating temperature as the dryer was heated and cooled, a low cycle fatigue analysis was performed to select a heating temperature considering an acceptable service life of the dryer. Considering the calculated fatigue life and working time, the dryer was designed with heating conditions to ensure a life of more than 1000 cycles.*

Keywords *- Thermal agitating dryer, Lithium Hydroxide, Direct heating method, Low cycle fatigue, Finite element analysis.*

1. Introduction

Agitated thermal dryers are used in various industries, including food processing, agriculture, mining, and secondary batteries. These devices use ribbons or paddles to agitate materials while applying external heat to remove moisture and ensure uniform cooling. Most drying processes adopt indirect heating methods, where external working fluids are heated, typically using oil for high temperatures above 100°C. However, indirect heating poses risks of fire and explosion due to high-temperature oil vapors if proper ventilation is not provided. In contrast, direct heating methods, using heating elements, offer a simpler structure and the ability to heat specific areas without the need for working fluids. To enhance safety and efficiency, a method using electric heater cables installed on the exterior of the casing has been introduced. This direct heating approach ensures fast heat transfer, is suitable for high-temperature operations, and optimizes energy usage while improving overall safety.

This study is on designing an agitating dryer used in the drying process to manufacture a cathode precursor for secondary batteries. The manufacturing process of cathode precursors for secondary batteries is divided into the co-precipitation method using sulfuric acid and the anhydrous lithium hydroxide production process using lithium hydroxide, with each process focusing on producing high-purity and high-quality precursors based on the chemical composition and reaction environment of the materials. In particular, dryers play a crucial role in removing moisture and ensuring uniform quality, thereby enhancing process efficiency and maximizing the final product's stability while optimizing energy consumption and productivity throughout the process.

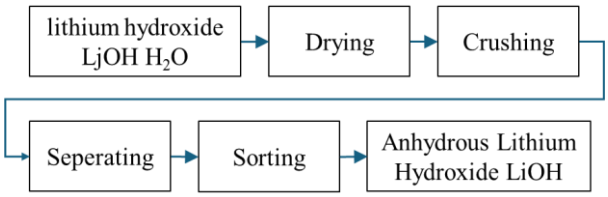

Fig. 1 General manufacturing anhydrous lithium hydroxide

In the general direct heating drying method, a wet material to be dried is fed into one end of a rotating drum and travels to the other end where it discharges as a dry product into a transfer conveyor. Heated air and some combustion gases are usually introduced into the dryer [1]. However, the direct heating method in this paper refers to a method in which a mineral insulation cable is attached to the outer wall of the casing, and the casing is heated using the conduction phenomenon, rather than a method in which a working fluid is heated to heat the dryer casing. Electric variables control the heating temperature of the mineral insulation cable. Regarding the variables for the heating temperature, Li et al. performed

insulated cable temperature calculation by a finite element analysis according to the current using [2]. Riba et al. proposed a model for the correlation between the current and temperature of insulated and jacketed cables in the air. They demonstrated through experiments and analyses that the temperature of the cable's conductor-insulation, insulation-jacket, and jacket-air sections can be precisely predicted [3]. Various studies have been conducted to expand the industrial applications of such mineral insulation cables [4-7].

The thermal dryer for manufacturing a cathode precursor for secondary batteries is a large-scale facility, and large deformation and local stress concentration may occur depending on the temperature distribution, which may cause plastic deformation. In order to prevent thermal shock of the material, the industrial drying operation is carried out by dropping the temperature below a certain temperature after drying and then repeatedly performing heating and drying. Therefore, a low-cycle fatigue analysis and a rupture analysis are required, considering the temperature of the areas where high deformation and stress are applied to the material used in the drying facility. The mechanical properties used in this paper are the mechanical and thermal property values disclosed in the ASME II Part D (2010) [8].

The heating temperature of the dryer can be as high as 350 °C, so mechanical properties for high-temperature fatigue properties are necessary. The low-cycle fatigue properties of the SS304 material at high temperatures were obtained from the report by Mei et al., who conducted a study on the material fatigue properties at room temperature, 300 °C, and 650 °C [9].

In this study, the goal was to predict the maximum allowable temperature and fatigue life to improve the facility efficiency in the design of the facility for drying a cathode precursor for secondary batteries. The temperature distribution of the heater during direct heating, as well as the deformation and stress at various locations, was predicted through finite element analysis, and the facility operating conditions for an acceptable fatigue life were determined through a low-cycle fatigue analysis.

2. Design of Direct Heating Thermal Dryer

In the direct heating of the thermal dryer, a mineral-insulated cable was employed as a heat source to increase the temperature of the casing surface of the heater. Since the operating temperature of the thermal dryer is 200 °C to 400 °C, a mineral insulated cable includes a copper-nickel inner conductor that can increase the temperature to the operating temperature, 97% MgO for insulation and 316 stainless as a sheath material. The heating temperature is 800 °C or higher, and it takes 15 minutes to heat to 980 °C and 5 minutes to cool down to room temperature. The heating cable was installed so as to make contact with the outer wall of the casing of the thermal heater. In order to uniformly increase the temperature of the casing, the heating cable layout was designed to have the densest spacings possible for installation. To ensure the homogeneity of the material being processed, the inside of the dryer was designed such that shovels rotate to agitate the material. Figure 2 shows the designed shape of the dryer and the agitator.

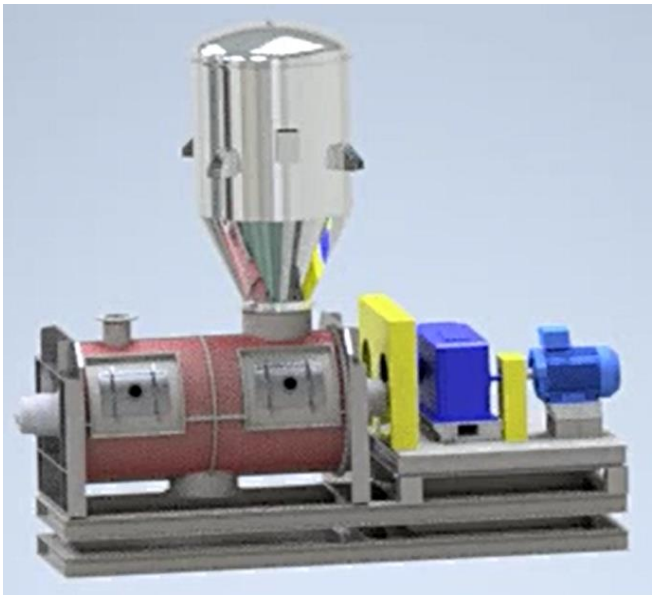

(a)

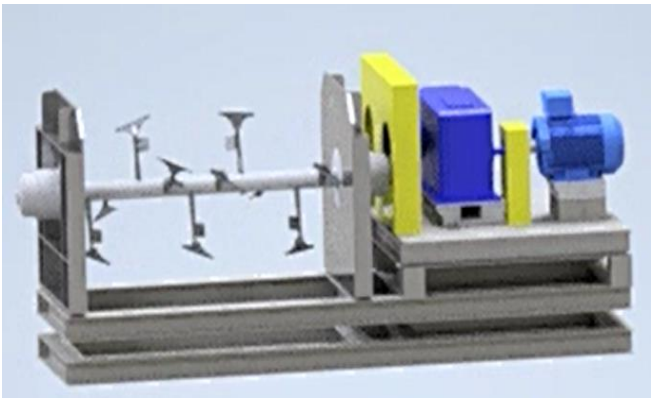

(b)

Fig. 2 Direct heating thermal dryer design (a) full model (b) Internal shoveling system for material agitation

The installation of the mineral-insulated cables for direct heating was designed with a 10 mm gap between cables, and the cables were installed to maintain the same gap on the cylindrical outer wall of the casing and both side plates.

The cables were installed in all areas except the window for material input and output, external operation checking in the casing, and the central area for installing the shovel drive shafts on both side plates. Figure 3 shows the cable installation layout in the casing and side plates.

In order to transfer the heat of the mineral-insulated cables to the material inside the casing through the casing and side plates, the outer wall was insulated using an insulating material.

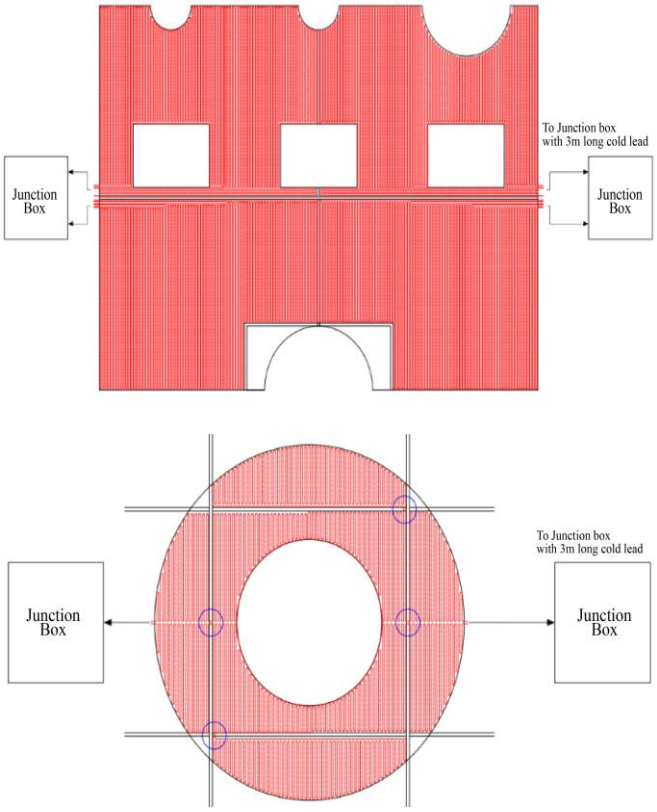

Fig. 3 Mineral insulated cable installation layout

3. Finite Element Analysis of Temperature and Stress of Thermal Dryer

3.1. Heating Conditions of Thermal Dryer

The dryer's heating for secondary batteries is a direct drying method in which the mineral-insulated cables are brought into contact with the casing for heating. The diameter of the mineral-insulated cables was Φ 4 mm, and the spacing between the cables was 10 mm. Since the diameter of the casing was Φ 2000 mm, when the heating boundary conditions are set to be the same as the actual ones, not only will the boundary conditions be very complicated, but the mesh will also be generated very densely, which may lengthen the analysis time. Therefore, the analytical conditions were simplified.

The casing and side plates of the thermal dryer may undergo deformation due to thermal expansion when heated to high temperatures, thereby causing plastic deformation in areas where the high stress exceeds the yield stress. The casing of the thermal dryer was made of SUS304 to withstand high-temperature deformation. The yield strength, tensile strength, elastic modulus, Poisson's ratio, density, and thermal properties such as thermal expansion coefficient and thermal conductivity of the SUS304 material according to temperature were obtained from the ASME data.

The change in the yield strength according to temperature shown in Figure 4 indicates that the material can easily undergo plastic deformation as the temperature increases.

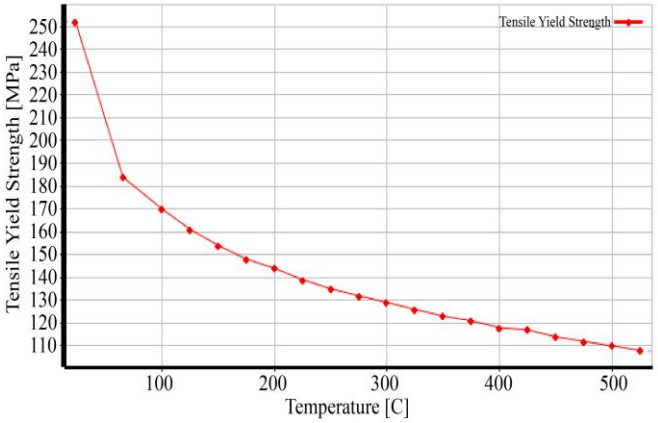

Fig. 4 Mechanical properties change with temperature

To simplify the heating conditions, analyses were performed under steady-state conditions to examine the feasibility of the simplification for three cases: a model in which the cables are installed in the same manner as in actual heating, a model in which the temperature is given at the points in contact with the cables; and a model in which the same temperature as the heating conditions is given to the entire surface.

The finite element analysis was performed using Ansys WB R2023. The analysis results for 3 cases are shown in Figure 5.

In addition, the contact heat transfer coefficient between the coil and the casing was set to be 10 W/mm^2°C, and the convective heat transfer coefficient by the air inside the casing was set to be 20 W/mm^2°C. In addition, since the part of the casing to be heated was cut out from the whole casing, a symmetric condition was applied so that no heat transfer occurred in the cut part.

According to the results of the steady-state analyses, the lowest temperatures for respective conditions were 295.85 °C, 294.96 °C, and 297.17 °C with a maximum deviation of 1.32 °C and a maximum temperature of 300 °C.

The edge model was excluded because the number of parts would be too many when applied to the full model, requiring a long analysis time and poor convergence. Therefore, considering that the deviation of 1.32 °C would not significantly affect the analytical results, face heating was selected as the boundary condition.

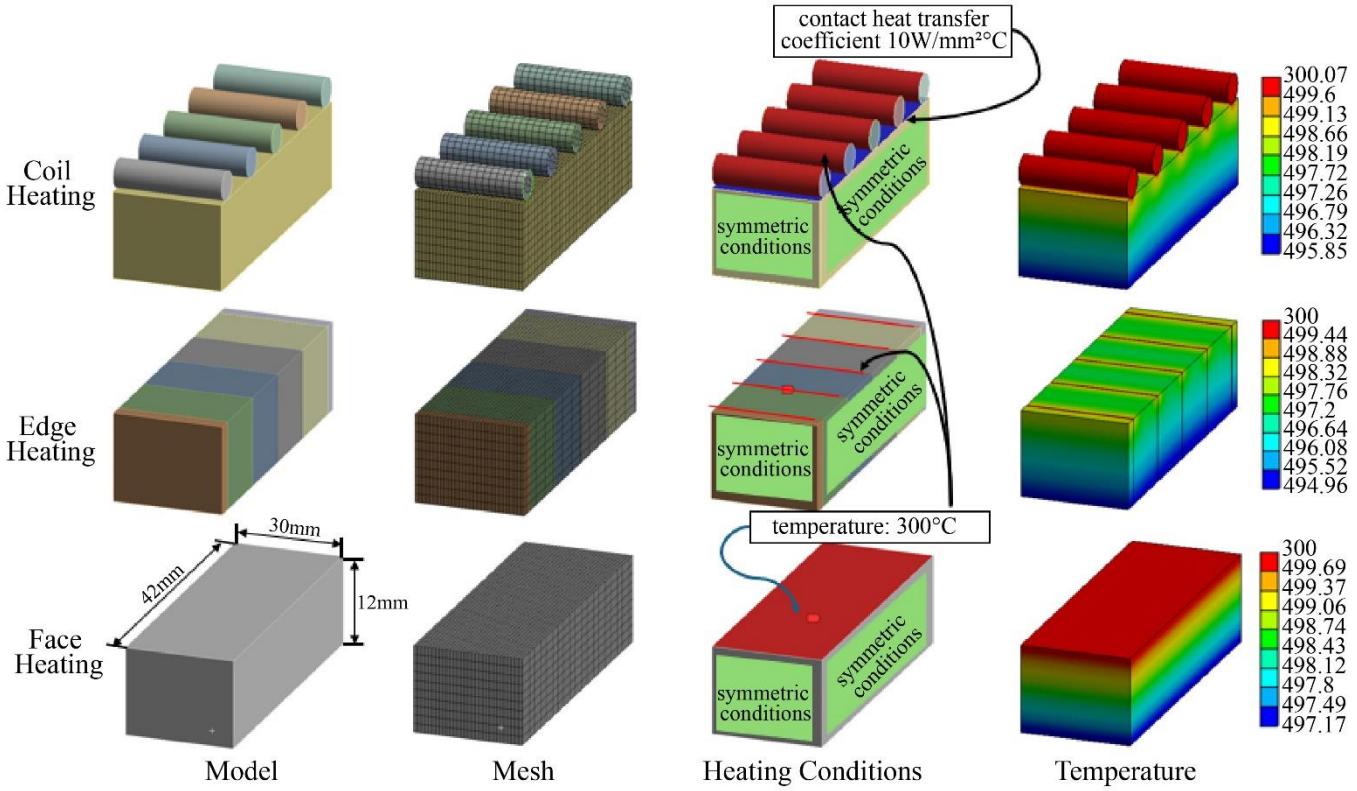

Fig. 5 Heat methodology comparison for mineral insulation cable heating

3.2. Temperature analysis of Direct Heating Dryer

The temperature difference by location, according to the temperature increase of the direct heating dryer, causes stress, depending on the amount of deformation of the dryer. Plastic deformation occurs locally when the stress exceeds the yield stress at an increased temperature.

In order to analyze the heating by the mineral-insulated cables of the heating dryer, it is necessary to predict the steady-state temperature and the heated-state stress of the casing that heats the material, both side plates, and the bearing area that supports the shaft in the heating dryer model shown in Figure 2.

In the model for the temperature analysis of the heating dryer, thermal input conditions are given to the casing that applies heat to both side plates, and heat dissipation plates attached to both side plates are assembled. For the grid generation in the finite element model, the casing was divided into a casing for drying the material, ribs for rigidity, a ring for assembling with the heat dissipation plates on both sides and a structure for loading and unloading the material was attached. Figure 6 shows the heating dryer model for the finite element analysis.

The mesh for the temperature analysis consisted of 461,264 hexahedral elements and 1,729,159 nodes. Figure 7 shows the mesh system for the temperature analysis.

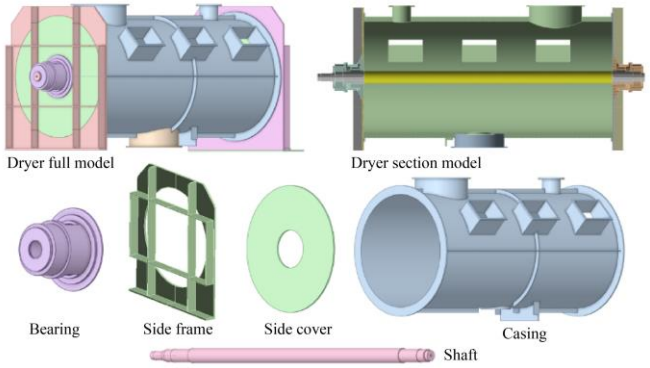

Fig. 6 Simplified dryer models for temperature analysis

The heating analysis of the dryer chamber was conducted by inputting heating temperatures of 250°C, 300°C, and 350°C on the surface where the mineral insulation cables are installed. These temperatures were selected to improve drying efficiency around the current operating condition of approximately 200°C, and the analysis was carried out for 250°C, 300°C, and 350°C. A heat transfer coefficient of 20 W/m²°C was applied as a boundary condition for convective heat transfer due to still air cooling, as air cooling occurs in the side frame. In the analytical model, the welded members were treated as an integrated body, and 1000 W/m²°C was applied to the components connected by bolts due to contact heat transfer at those points [10,11].

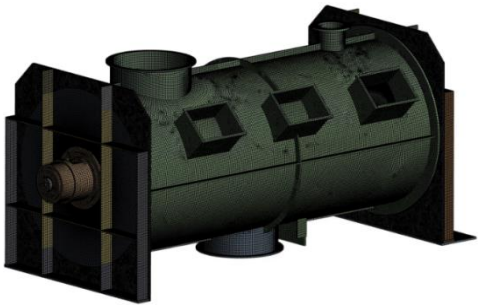

Fig. 7 Mesh system for temperature analysis

External heat transfer was not considered since an insulation cover is installed on the casing and the side plates where heating occurs to prevent the heating energy from being lost. Figure 8 shows the boundary conditions for the temperature analysis.

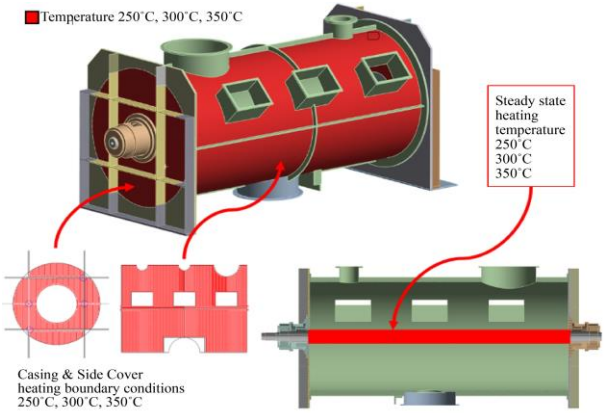

(a)

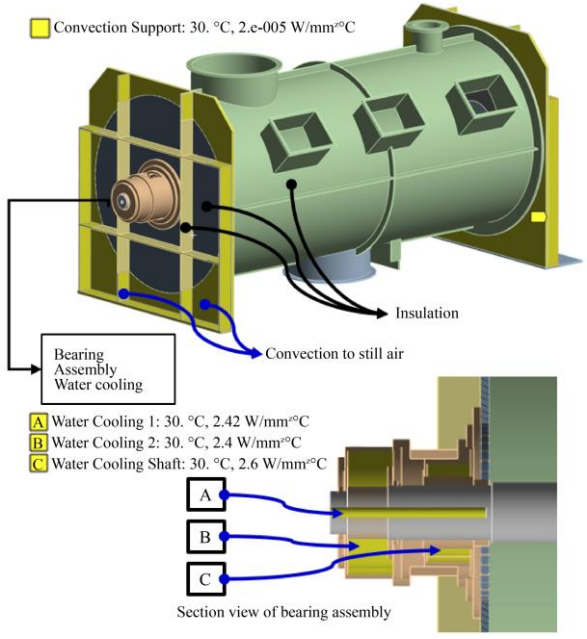

(b)

Fig. 8 Boundary conditions for temperature analysis (a) heating boundary conditions (b) cooling boundary conditions

The steady-state temperature distributions in the casing and the side plates, when the electric dryer was heated to 250 °C, 300 °C, and 350 °C, were analyzed using Ansys WB R2024. The temperature on both side plates where the heat source was applied decreased due to convection into the air, but the insulated casing area maintained a high temperature.

The maximum temperatures in the casing were 251.99 °C, 301.67 °C, and 351.92 °C, which were a little higher than the heating temperature, and the minimum temperatures were 29.5 °C, 29.94 °C, and 29.99 °C at the side frame. Figure 9 shows the temperature distribution of the dryer obtained through the temperature analysis.

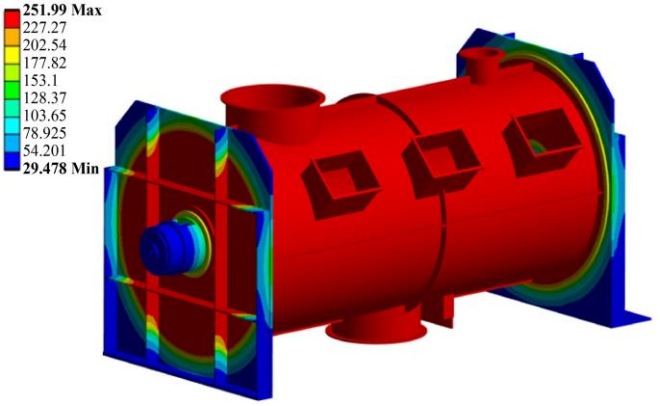

(a)

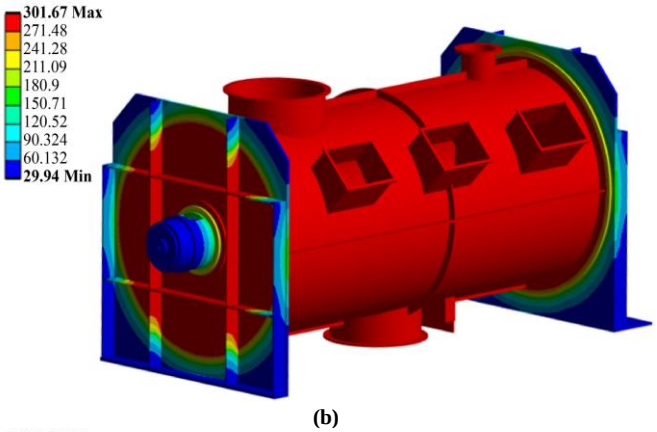

(b)

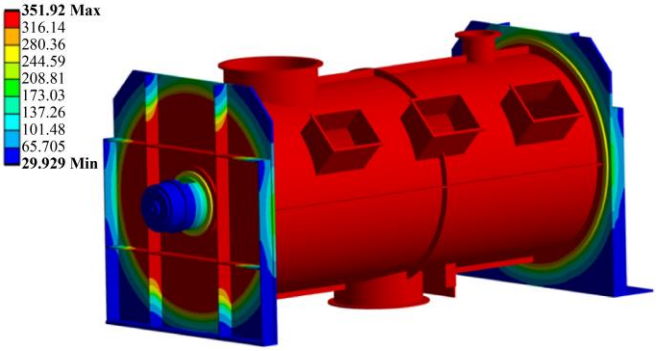

(c)

Fig. 9 Steady state temperature distribution by FE analysis (a) 250°C, (b) 300°C and (c) 350°C heating conditions

3.3. Deformation and Stress Analysis on Heating

As the temperature of the casing of the dryer is increased, thermal expansion occurs in the casing and on the side plates, and the stress distribution will be formed accordingly. The deformation of the dryer due to heating was analyzed by inputting the temperature distribution, which is the result of the temperature analysis by Ansys WB, as input information to the Ansys WB Mechanical module. The boundary conditions for the deformation analysis were as follows: the bottom surface of one side plate of the thermal dryer was fixed in the x, y, and z directions; a friction coefficient of 0.1 was applied to the lower part of the opposite side plate, and the gravity was applied to all the components so that their self-weight acted in the opposite direction to the y direction. Figure 10 shows the boundary conditions for the deformation analysis.

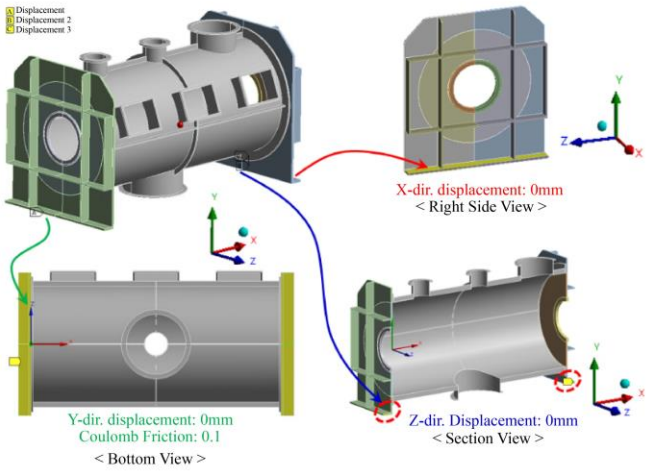

Fig. 10 boundary conditions for stress and deformation FE analysis

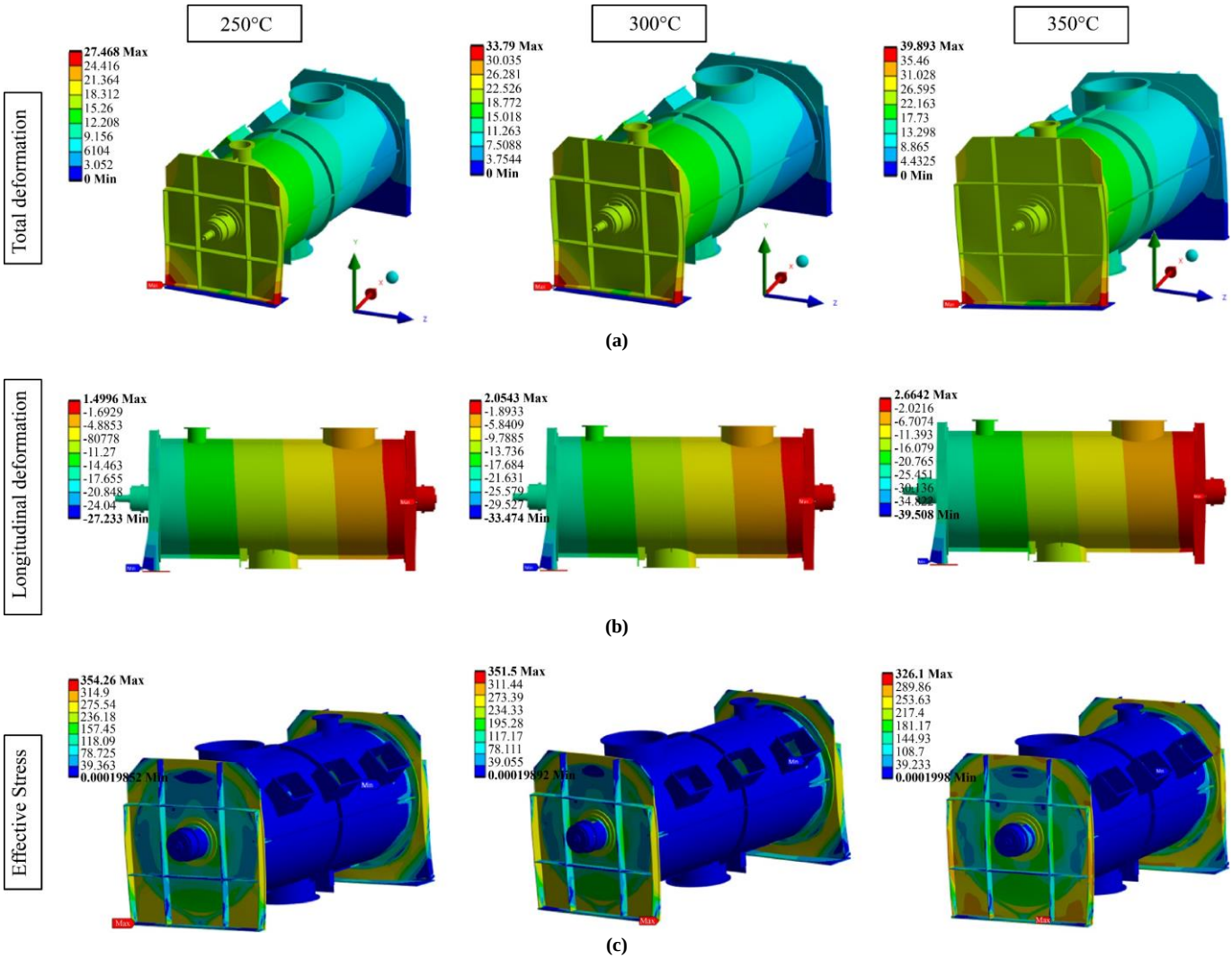

Fig. 11 Stress and temperature distribution of dryer components (a) Total deformation, (b) deformation of the longitudinal direction, (c) Effective stress

As shown in Figure 11(a), when the steady-state temperatures of 250 °C, 300 °C, and 350 °C were reached by heating, the maximum deformation was 27.4468 mm, 33.79 mm, and 39.893 mm, respectively. As shown in Figure 11(b), the maximum longitudinal deformation due to heating was the same as the maximum total deformation. As shown in Figure 11(c), the maximum stress applied to the side frame due to heating was 354.26 MPa, 351.5 MPa, and 326.1 MPa depending on the heating temperature. As confirmed in Figure 9, the area where the maximum stress was generated exhibited a temperature close to room temperature.

When the heating was performed to 250 °C to 350 °C, the maximum stress applied was 326 to 354 MPa. When considering the temperature of the area where the maximum stress was applied, it can be seen that plastic deformation occurred with reference to the change in the yield strength by temperature shown in Figure 4. Therefore, since the heating dryer undergoes the operation of drying the material and then repeated cooling of the material to room temperature and reheating thereof, it is necessary to predict the fatigue life of the dryer in consideration of the strain and temperature of each component when heated to the drying temperature.

3.4. Fatigue life calculation of Thermal Dryer

The low-cycle fatigue theory can calculate the fatigue life when plastic deformation occurs repeatedly. Since the present study involves a calculation of fatigue life considering the stress and strain that are exhibited in the steady-state high-temperature range, the fatigue life was calculated by formulating the coefficients of Table 1 of the Basquin and Manson-Coffin Model shown in Equation (1) for the SS304 material at room temperature, 300 °C, and 650 °C with the heating temperature as a variable, as performed by Mei et al. [9].

$$\frac{\Delta\varepsilon}{2} = \frac{\Delta\varepsilon_e}{2} + \frac{\Delta\varepsilon_p}{2} = \frac{\sigma_f'}{E}(2N_f)^b + \varepsilon_f'(2N_f)^c \quad (1)$$

Table 1. Cycle stress-strain properties of SS304 at RT, 300℃ and 650℃ [9]

Temperature [℃]	σf′ [MPa]	εf′	b	c	R^2
RT	768.36	3.25	-0.09	-0.19	0.87
300℃	660.17	2.43	-0.11	-0.16	0.98
650℃	424.68	5.09	-0.08	-0.29	0.76

The fatigue life was predicted using the Basquin and Manson-Coffin Model, considering the stress and strain acting on the components according to the heating temperature. In order to calculate the fatigue life by considering the steady-state temperature at the point where the maximum stress and maximum strain act on each component, the locations of the maximum stress and maximum strain on five components, the casing, casing rib, side rib, support frame, and bearing and shaft, were analyzed at 300 °C, and the results are shown in Figure 12. The temperature at the points where each component's maximum stress and maximum strain occurred is indicated at the lower right of Figure 12. For the casing, casing rib, side rib, and bearing and shaft, the locations of the maximum stress and those of the maximum strain were different, but for the support frame, the locations were the same.

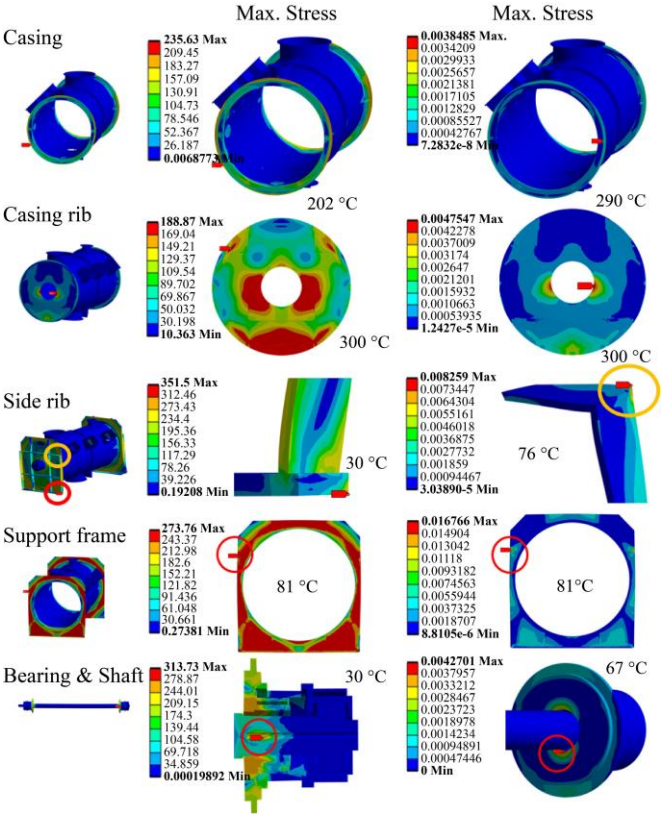

Fig. 12 Maximum stress and strain location of each component at 300℃ heating conditions

For the representative heating temperature of 300 °C, Table 2 summarizes the stress, strain, and temperature at the locations where the maximum stress and the maximum strain were exhibited at each component and the fatigue life calculated by using the Basquin and Manson-Coffin Model of Equation (1) and the coefficient change by temperature in Table 1 obtained using a regression equation. The minimum fatigue life was found at the rib end of the support frame, and the fracture risk was predicted after 1,145 cycles.

For the representative heating temperature of 300 °C, Table 2 summarizes the stress, strain, and temperature at the locations where the maximum stress and the maximum strain were exhibited at each component and the fatigue life calculated by using the Basquin and Manson-Coffin Model of Equation (1) and the coefficient change by temperature in Table 1 obtained using a regression equation. The minimum fatigue life was found at the rib end of the support frame, and the fracture risk was predicted after 1,145 cycles.

Table 2. Fatigue life calculation of maximum stress and strain location of 300℃ heating conditions

Component	Class.	Stress [MPa]	Strain	Temp [℃]	Fatigue life [Cycles]
Casing	Max. Stress	215,63	0.0011	202	12.5E+9
	Max. Strain	179.92	0.0038	290	8,026,000
Casing rib	Max. Stress	203.8	0.0009	300	69.5E+9
	Max. Strain	183.00	0.0047	300	2,236,426
Side rib	Max. Stress	351.50	0.0018	30	179.1E+6
	Max. Strain	266.14	0.0082	76	65,090
Support frame	Max. Stress	273.76	0.0167	81	1,145
	Max. Strain	273.76	0.0167	81	1,145
Bearing & shaft	Max. Stress	313.72	0.0015	30	473.3E+6
	Max. Strain	262.32	0.0042	67	2,702376

Table 3. Fatigue life comparison of different heating temperatures

Component	Class.	250℃ Fatigue life [Cycles]	300℃ Fatigue life [Cycles]	350℃ Fatigue life [Cycles]
Casing	Max. Stress	5.8E+9	12.5E+9	9.2E+9
	Max. Strain	35.7E+6	8,026,000	753,860
Casing rib	Max. Stress	13.0E+9	69.5E+9	2.0E+9
	Max. Strain	15.6E+6	2,236,426	462,429
Side rib	Max. Stress	182.1E+6	179.1E+6	243.0E+6
	Max. Strain	541,567	65,090	2.6E+9
Support frame	Max. Stress	4,795	1,145	450
	Max. Strain	4,795	1,145	450
Bearing & shaft	Max. Stress	179.1E+6	473.3E+6	684.0E+6
	Max. Strain	2.9E+6	2,702376	186,591

Table 3 shows the fatigue life of each component at different heating temperatures of 250 °C, 300 °C, and 350 °C. The side frame also exhibited the shortest fatigue life at the heating temperatures of 250 °C and 350 °C. This may be because the side frame is located between the high-temperature casing and casing rib and the low-temperature side rib. So, the occurrence of the plastic deformation of the component decreases its fatigue life. The predicted fatigue life of the support frame was 4,795 cycles at 250 °C, 1,145 cycles at 300 °C, and 450 cycles at 350 °C.

4. Conclusion

The design of a high-efficiency agitation dryer required for the manufacturing process of lithium hydroxide, a cathode material for secondary batteries, was carried out. The dryer of the present study is a direct heating dryer using mineral insulation cables, and the same heating conditions as actual heating require excessive analysis time due to their contact with the grid. A case study was conducted on an effective heat input method to replicate the same heat input conditions and a similar temperature distribution as the actual scenario, confirming that acceptable results can be achieved by applying the heating temperature on the surface where the mineral insulation cables are installed.

The steady-state temperature distribution when heated to 250 °C, 300 °C, and 350 °C showed that the maximum temperatures were a little higher than the heating temperatures, but the temperature distribution on the side frame was similar under the three heating conditions because of the cooling by the heat dissipation plates.

When the steady-state temperatures of 250 °C, 300 °C, and 350 °C were reached, the maximum deformation was 27.4 mm, 33.8 mm, and 39.9 mm, and the maximum stress was 354.3 MPa, 351.5 MPa, and 326.1 MPa, respectively, indicating that as the temperature increases, the deformation increases and the stress decreases.

As the yield stress is exceeded and plastic deformation occurs when heated to a high temperature, low-cycle fatigue may occur when the drying operation is repeated. Therefore, the fatigue life for each of the three temperatures was calculated, and the results showed that the fatigue life was shortest at the side from, which connects components with a rapid temperature change between. Since the fatigue life was as low as 450 cycles when the heating temperature was 350 °C, the heating temperature may need to be controlled below 300 °C. The results will be compared with the currently operating equipment in the future, and further analysis will be conducted to identify and determine the optimal operating conditions.

References

[1] Arun S. Mujumdar, *Handbook of Industrial Drying*, 4th ed., CRC Press, pp. 1-1348, 2006. [Google Scholar] [Publisher Link]

[2] Xin-jian Li et al., "Insulated Cable Temperature Calculation and Numerical Simulation," *MATEC Web of Conferences*, vol. 175, pp. 1-3, 2018. [CrossRef] [Google Scholar] [Publisher Link]

[3] Jordi-Roger Riba, and Jordi Llauradó, "A Model to Calculate the Current–Temperature Relationship of Insulated and Jacketed Cables," *Materials*, vol. 15, no. 19, pp. 1-16, 2022. [CrossRef] [Google Scholar] [Publisher Link]

[4] N.R. Rafferty et al., "Considerations for Application of Mineral Insulated Electrical Resistance Heating Cable," *Record of Conference Papers Industry Applications Society 52nd Annual Petroleum and Chemical Industry Conference*, Denver, CO, USA, pp. 103-111, 2005. [CrossRef] [Google Scholar] [Publisher Link]

[5] Jin Tong Hu et al., "Analysis of Heating Scheme of Mineral Insulated Cable Tubing-Casing Annular in Ultra-Deep Heavy Oil Well," *Advances in Energy Resources and Environmental Engineering*, pp. 1369-1377, 2024. [CrossRef] [Google Scholar] [Publisher Link]

[6] HongWei Zhang et al., "Comparative Analysis of Mineral Insulated Cable Heating Schemes in Ultra-deep Heavy Oil Wells," *2022 2nd International Conference on Electrical Engineering and Control Science (IC2ECS)*, Nanjing, China, pp. 1106-1109, 2022. [CrossRef] [Google Scholar] [Publisher Link]

[7] Susrutha Biswas, "Cultivating Localization: Adapting Mineral Insulated Cable for Indigenous Heater Applications," *The American Journal of Interdisciplinary Innovations Research*, vol. 5, no. 9, pp. 1-5, 2023. [Google Scholar] [Publisher Link]

[8] "ASME Boiler and Pressure Vessel Code, Section II (Material)," *The American Society of Mechanical Engineers*, pp. 1-19, 2019. [Google Scholar] [Publisher Link]

[9] Ting Mei et al., "The Low-Cycle Fatigue Behavior, Microstructure Evolution, and Life Prediction of SS304: Influence of Temperature," *Materials*, vol. 16, no. 18, pp. 1-19, 2023. [CrossRef] [Google Scholar] [Publisher Link]

[10] Junjia Cui et al., "Predictions of the Mechanical Properties and Microstructure Evolution of High Strength Steel in Hot Stamping," *Journal of Materials Engineering and Performance*, vol. 21, pp. 2244-2254, 2012. [CrossRef] [Google Scholar] [Publisher Link]

[11] Heung-Kyu Kim, Seong Hyeon Lee, and Hyunjoo Choi, "Evaluation of Contact Heat Transfer Coefficient and Phase Transformation during Hot Stamping of a Hat-Type Part," *Materials*, vol. 8, no. 4, pp. 2030-2042, 2015. [CrossRef] [Google Scholar] [Publisher Link]